Electronic structure, bonding, and ground-state properties of AlB_2-type transition-metal diborides

P. Vajeeston,[1,2] P. Ravindran,[1] C. Ravi[1,*], and R. Asokamani[1]
[1]*Department of Physics, Anna University, Chennai-25, India*
[2]*Department of Chemistry, University of Oslo, Box 1033, Blindern, N-0315, Oslo, Norway*
(Received 29 July 2000; published 9 January 2001)

The electronic structure and ground state properties of AlB_2 type transition metal diborides TMB_2 (TM=Sc, Ti, V, Cr, Mn, Fe, Y, Zr, Nb, Mo, Hf, Ta) have been calculated using the self consistent tight-binding linear muffin-tin orbital method. The equilibrium volume, bulk moduli (B_0), pressure derivative of bulk moduli (B_0'), cohesive energy (E_{coh}), heat of formation (ΔH), and electronic specific heat coefficient (γ) are calculated for these systems and compared with the available experimental and other theoretical results. The bonding nature of these diborides is analyzed via the density of states (DOS) histogram as well as the charge density plots, and the chemical stability is analyzed using the band filling principle. The variation in the calculated cohesive properties of these materials is correlated with the band filling effect. The existence of a pseudogap in the total density of states is found to be a common feature for all these compounds. The reason for the creation of the pseudogap is found to be due to the strong covalent interaction between boron *p* states. We have made spin polarized calculations for CrB_2, MnB_2, and FeB_2 and found that finite magnetic moments exist for MnB_2 and CrB_2 whereas FeB_2 is nonmagnetic.

DOI: 10.1103/PhysRevB.63.045115 PACS number(s): 71.20.−b, 64.30.+t, 75.10.Lp

I. INTRODUCTION

The modern scientific and technical revolution is responsible for increasing interest and impetus in the search for materials possessing specific and desired properties. The transition metal borides can be classified as highly refractory and corrosion-resisting compounds,[1] and the transition metal compound ($Nd_2Fe_{14}B$) has been recently applied as a high-performance permanent magnetic material. From a more scientific point of view, the monoborides have INVAR behavior,[2] while the diborides of transition metal have a unique combination of properties such as high melting point, hardness, chemical stability, high thermal conductivity, low electrical resistivity, and low work function.[3] Since this combination is markedly different from that of parent materials, a great deal of research has been devoted to investigating the interaction between boron and the metal atoms.[3,4] Especially the TiB_2 compound is a potential despersoid for the development of light-weight high-temperature structural materials. These AlB_2-type transition metal diborides have attracted researchers from different fields and many experimental[5–7] as well as theoretical studies are going on in these materials.[8–11] Although a number of excellent research works have been published on the structure and physical properties of the borides,[12–14] the bonding nature of these compounds is not very clear yet.[12] So, we have tried to explain the bonding nature with density-of-states (DOS) histogram and charge density plots. Recently, band structure calculations have been performed on AlB_2-type compounds by Wang *et al.*,[12] in which they have explained the chemical stability of these AlB_2-type diborides in terms of band filling principle.[12] In the present work, the chemical stability is explained in terms of the band filling principle and also by the density of states at the Fermi level $N(E_F)$. Though the electronic specific heat coefficient γ for these compounds had been reported by others,[12,15] the results of the present theoretical work are more reliable because the calculations are performed through *k*-point optimization procedure. The bulk modulus B_0 of these compounds are also calculated and these B_0 values are compared with the available experimental[16] and theoretical[17,18] values.

As there are no reported theoretical values of heat of formation (ΔH) for these compounds, an attempt is made to theoretically calculate ΔH values which are compared with the available experimental values.[19] We have made spin-polarized calculations for FeB_2, CrB_2, and MnB_2 compounds. Mohn *et al.*[14,20,21] have made theoretical studies on magnetic properties of mono-, semi-, and diborides using the augmented spherical wave (ASW) method. We compare our results with their results and also with other experimental[22] results.

We present the results of the local-density approximation (LDA) based investigation, using the self-consistent tight binding-linear muffin-tin orbital (TB-LMTO) method. The rest of this paper is organized in the following way. In Sec. II, the crystallographic structures of these transition metal diborides are explained. In Sec. III, the details of the calculations are presented. The total and site projected density of states (DOS) for all the compounds are reported in Sec. IV. In Sec. V the nature of chemical bonding is analyzed with the help of charge density plots. Cohesive properties for all the compounds are given in Sec. VI. In Sec. VII, the chemical stability of these systems is explained. The magnetic properties of the MnB_2 and CrB_2 are explained in Sec. VIII. A summary of the results is given in the last section.

II. THE STRUCTURAL ASPECTS OF THE TRANSITION METAL DIBORIDES

The crystal structure of AlB_2-type transition metal diborides is designated as $C32$ with the space group symmetry $P6/mmm$. It is simply a hexagonal lattice in which close-packed TM layers are present alternative with graphite-like B layers. These diborides cannot be exactly layered compounds because the interlayer interaction is strong even though the TM layers alternate with the B layers in their crystal struc-

TABLE I. The calculated and experimental lattice parameters (a,c in Å), equilibrium volume (in Å^3/atom), the TM-B and B-B bond distance (in Å) for TMB_2 compounds.

Compound	Present		Experimental		Volume	TM-B	B-B
	a	c	a	c			
ScB_2	3.154	3.523	3.148	3.516	10.115	2.533	1.821
TiB_2	3.070	3.262	3.038	3.22	8.876	2.409	1.773
VB_2	2.983	3.047	2.998	3.056	7.825	2.297	1.722
CrB_2	2.949	3.045	2.969	3.066	7.642	2.284	1.703
MnB_2	2.924	2.950	3.009	3.039	7.281	2.242	1.688
FeB_2	2.931	2.921	3.045	3.035	7.242	2.235	1.674
YB_2	3.314	3.855	3.290	3.835	12.223	2.716	1.914
ZrB_2	3.197	3.561	3.170	3.533	10.502	2.564	1.846
NbB_2	3.107	3.328	3.115	3.265	9.271	2.447	1.794
MoB_2	3.081	3.101	3.041	3.066	8.495	2.359	1.779
HfB_2	3.166	3.499	3.139	3.473	10.124	2.530	1.828
TaB_2	3.115	3.244	3.294	3.886	9.085	2.421	1.799

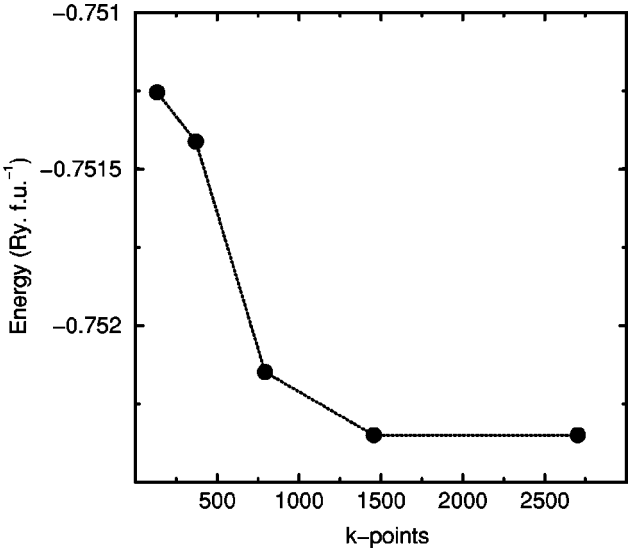

FIG. 1. Total energy vs number of k points in TiB_2.

ture. The boron atoms lie on the corners of hexagons with three nearest neighbor boron atoms in each plane. The TM atoms lie directly in the centers of each boron hexagon, but midway between adjacent boron layers; each TM atom has 12 nearest neighbor B atoms, six nearest neighbor in plane TM atoms. There is one formula unit per primitive cell and the crystal has simple hexagonal symmetry (D_{6h}), whose crystal structure and Brillouin zone are found in earlier publications.[22–25] By choosing appropriate primitive lattice vectors, the atoms are positioned at TM (0,0,0), B ($\frac{1}{3},\frac{1}{6},\frac{1}{2}$), and B ($\frac{2}{3},\frac{1}{3},\frac{1}{2}$) in the unit cell. The distance between TM–TM is equal to **c**. This structure is quite close packed, and can be coped with efficiently and accurately by the atomic sphere approximation (ASA) method.[26–29] The valence states considered in the present calculation for the boron atoms are $2s$, $2p$, and $3d$ and for the transition metals are $3d$, $4s$, and $4p$ for the first series, $4d$, $5s$, and $5p$ for the second series and $5d$, $6s$, and $6p$ for the third series. The crystallographic parameters of TMB_2 compounds used in the present calculations are listed in Table I.

III. METHOD OF COMPUTATION

To calculate the electronic ground-state properties of the transition-metal diborides, we have used the TB-LMTO method of Andersen.[27,28] The von Barth–Hedin[30] parametrization is used for the exchange correlation potential within the local density approximation. The LDA theory has been shown by many researchers during the past few decades to give accurate ground-state properties such as equilibrium volume, cohesive energies of elements and solids, bulk modulus, heat of formation, and electronic specific heat coefficient of intermetallic compounds.[31–34] In the present calculation, we have used ASA. In this approximation, the crystal is divided into space filling spheres, and therefore with slightly overlapping spheres centered on each of the atomic sites. In all our calculations reported here, the Wigner–Seitz (WS) sphere radii are such that an overlap is below 9%. The average WS radius was scaled so that the total volume of all the spheres is equal to the equilibrium volume of the unit cell. The calculations are semirelativistic, i.e., except spin-orbit coupling, all the other relativistic effects are included. The combined correction terms are also included in the calculation. The Brillouin zone k-point integrations are made using the tetrahedron method on a grid of 1456k points in the irreducible part of the hexagonal Brillouin zone (IBZ), which corresponds to 27 000 k points throughout the Brillouin zone. The optimized k points versus energy of TiB_2 is shown in Fig. 1. We find that above 1456 k points the energy becomes constant. So, in all our calculations, we use 1456 k points in the IBZ. We have used optimized c/a and equilibrium volume obtained from our calculations for the cohesive properties study. The calculations are done at different cell volumes for each system and the corresponding total energies are evaluated self-consistently by iteration to an accuracy of 10^{-6} Ry. For the borides which possess Cr, Mn, or Fe as one of the constituents, we have made spin polarized calculation to look for spontaneous magnetization.

IV. DENSITY OF STATES

The site projected and total density of states (DOS) of TMB_2 are shown in Figs. 2 and 3 where the vertical line indicates Fermi level E_F. The DOS histogram of TMB_2 consists of three parts: (a) the peak present in the lower energy part of the DOS curve which is mainly due to the localized or tightly bound s electrons of B; (b) the bonding states of TM-d and B-$2p$ orbitals near the Fermi level; and (c) the top of the DOS curve due to antibonding states. It is found that the B-s electrons in TMB_2 are localized and naturally its effect in bonding is very small. The electrons from TM-d and the B-$2p$ states both contribute to the density of states at the Fermi level. The DOS of TM-d and B-$2p$ are energetically degenerate from the bottom of the valence band to the Fermi level, indicating the possibility of covalent bonding

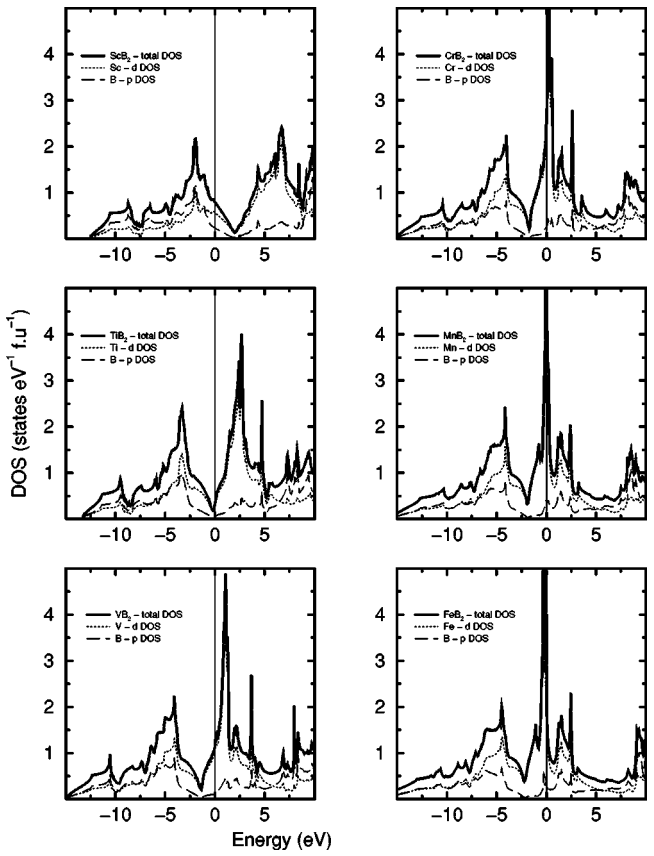

FIG. 2. Total and site projected density of states for $3d$ transition metal diborides ScB_2, TiB_2, VB_2, CrB_2, MnB_2, and FeB_2.

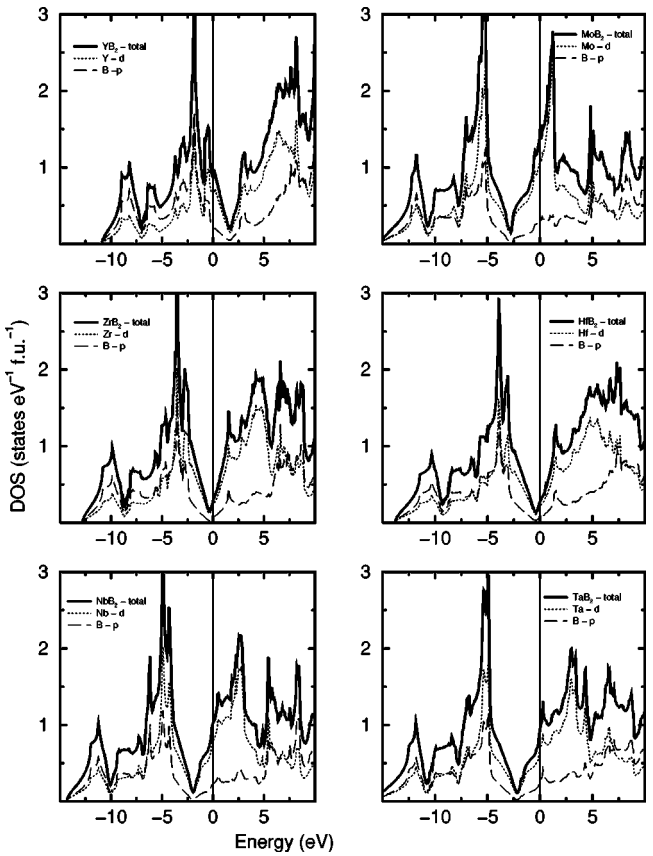

FIG. 3. Total and site projected density of states for YB_2, ZrB_2, NbB_2, MoB_2, HfB_2, and TaB_2.

between TM and B atoms in all these compounds. However, the spatial separation between TM and B species and the charge transfer effect prevent the hybridization effect. As a result, our charge density studies show that the bonding between TM and B atoms in early transition metals diborides are not dominated by covalent bonding.

From the DOS curves given in Figs. 2 and 3, it is clear that these compounds have close similarity. Further, all these compounds possess finite $N(E_F)$ at the Fermi level. Hence, these diborides are said to exhibit metallic behavior in their crystalline state. From our detailed investigation of charge density distribution between various atoms in TMB_2 compounds we found that the metallic bonding between TM is the principal cause for the metallicity in these compounds. From the DOS histogram we found that the *d*-DOS bonding state peak is systematically shifting towards the lower energy side as one moves from Sc to Fe, Y to Mo, and Hf to Ta in the $3d$, $4d$, and $5d$ transition metal series respectively due to increase in the number of valence electrons (see Figs. 2 and 3). Although the rigid-band model describes the electronic structures of these diborides fairly well, there are some differences between the band structures as expected. The density of states is largest towards the end of a transition metal series because the antibonding states at the top of the *d* band are the most localized *d* states. These antibonding states have the smallest interaction with the neighboring atoms and hence, the smallest energy spread. The height of the DOS peak is lower in the $4d$ series TMB_2 compounds than the $3d$ series because the $4d$ orbitals extend further from the nucleus than the $3d$ orbitals. Since there is no sizable increase in the atomic volumes of the $4d$ series TMB_2 compounds compared to the corresponding $3d$-series TMB_2 compounds, the $5d$ and $4d$ orbitals on neighboring atoms must overlap more than do the $3d$ orbitals. This increased overlap leads to a larger interaction between neighbors, and thus to a larger bandwidth and a smaller density of states.

The typical feature of the total DOS of these compounds is the presence of what is termed as a pseudogap (a sharp valley around the Fermi energy) in all these compounds. It is interesting to note that pseudogaps exist not only in crystalline solids[35] and amorphous alloys,[36] but also in quasicrystals.[37] Two mechanisms were proposed for the formation of pseudogap in the binary alloys. One is of ionic origin and the other is owing to hybridization effects. The electronegativity difference between TM and B is low and hence the ionicity does not play a major role on bonding behavior of these compounds (the percentage of ionicity is less than 8% in these compounds). Consequently the pseudogap present in TMB_2 is believed to be due to covalent hybridization between TM and B atoms. Such a strong hybridization gives not only an important mixing between the states of the conduction bands but also leads to a separation of the bonding states creating a pseudogap. The pseudogap is also observed in all hexagonal-close-packed (hcp) transition metals[38] and this is attributed to *d* resonance. The formation of pseudogap in TiB_2 was believed to be due to the compe-

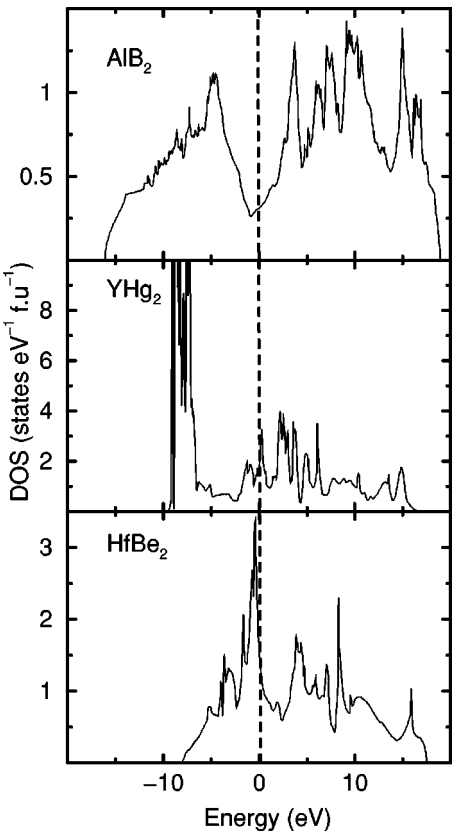

FIG. 4. Total density of states for AlB_2, YHg_2, and $HfBe_2$ in the AlB_2 structure.

tition between the strong Ti-B hybridization and the Ti $3d$ resonance.[10] Our charge density distribution plots show that there is weaker hybridization between TM and boron atoms in the early TM diborides even though they possess pseudogap feature. This indicates that, apart from TM-B covalent hybridization, some other factor influences the creation of pseudogap in these compounds. In order to identify the origin of the pseudogap feature in all these compounds, we have made model calculations for compounds with same structures. The total DOS curves for AlB_2, YHg_2, and $HfBe_2$ in the AlB_2 structure are shown in Fig. 4. Interestingly, the pseudogap is present in AlB_2 also even though it does not have any p-d covalent interaction. Furthermore, the DOS of YHg_2 does not show a pseudogap feature even though it has TM–TM bond. Another example is $HfBe_2$, it has Hf(d)–Hf(d) interaction as well as Be(s)–Be(s) interaction. From Fig. 4, it should be noted that there is no noticeable pseudogap present in $HfBe_2$. So, we conclude that the presence of pseudogap in AlB_2-type transition metal diborides is mainly originating from B(p)–B(p) covalent interaction and the TM–TM or TM–B covalent interactions are less significant to the creation of pseudogap. It should be noted that the E_F is lying on the pseudogap in TiB_2, ZrB_2, and HfB_2. This is due to the band filling effect since all these three compounds possess same number of electrons per atom.

V. CHARGE DENSITY AND BONDING

On the basis of Korringa-Kohn-Rostoker (KKR) calculations and the x-ray photoelectron spectrum, Ihara, Hirabayashi, and Nakagawa[24] proposed that the bonding nature of ZrB_2 can be explained by a combination of the graphite bonding model of the boron network and the hcp metal bonding model of zirconium. A tight-binding calculation for TiB_2 was performed by Perkins and Sweeney[25] and found strong evidence of graphite band structure. From the viewpoint of orbital overlap, Burdett, Lanadell, and Miller[13] studied the electronic structure of transition metal borides with the AlB_2 structure and found that the interaction of the orbitals of the transition metal with those of the planar graphite-like net of boron atoms and interaction with those of other metals are both important in influencing the properties of these compounds. Tian and Wang,[10] from their electronic structure studies, found that strong interlayer bonding plays an important role in the formation of TiB_2. The anisotropy in the bonding behavior of TiB_2 has been studied recently using the orientation-dependent electron-energy-loss spectroscopy along with the band structure calculations.[39] The nature of the bonding in transition metal diborides has been described in early works by simplified models which emphasize the role of TM-TM bonding,[40,41] B-B bonding,[42,43] or TM-B bonding.[44–47] These approaches are not consistent with each other. Further, two conflicting points of view have been advanced regarding the electronic structure and chemical bonding in transition-metal borides. In some studies, it has been assumed that there is electron transfer from boron to the metal[41,48,49] while in others it is argued that charge transfer is in the opposite direction.[43,50–54] Moreover, the conclusions arrived at regarding the nature of chemical bonding in diborides from electronic structure calculations are also contradictory to each other.[55,56] So, in order to have deeper understanding about the origin of bonding behaviors in AlB_2 transition metal diborides, we have given the three dimensional view of charge density distribution for TiB_2 in different planes where Ti-Ti, B-B, and Ti-B bondings are present in Figs. 5(a), 5(b), and 5(c), respectively. From Fig. 5(a), it is clear that the Ti-Ti bonding in TiB_2 is not dominantly of covalent nature. Instead we found finite uniformly distributed charge density between Ti atoms as shown in Fig. 5(a) indicating that there is a metallic bonding between Ti-Ti in TiB_2. To have better understanding about the nature of bonding between boron atoms, the charge density distribution in the (0002) plane of TiB_2 is given in Fig. 5(b). From this figure, it is clear that there is strong covalent interaction between boron atoms in TiB_2. The observation of strong covalent bonding between boron atoms is consistent with experimental studies in the sense that the thermal expansion coefficient measurements on TMB_2 compounds show[57] that the thermal expansion coefficient in the **c** direction decreases with increasing radius of the metal atom and that in the **a** direction changes very little with the size of the metal radius. The charge density distribution between Ti and B atoms in TiB_2 is shown in Fig. 5(c). From this figure the Ti atoms are chosen to be in the origin. It should be noted that there is

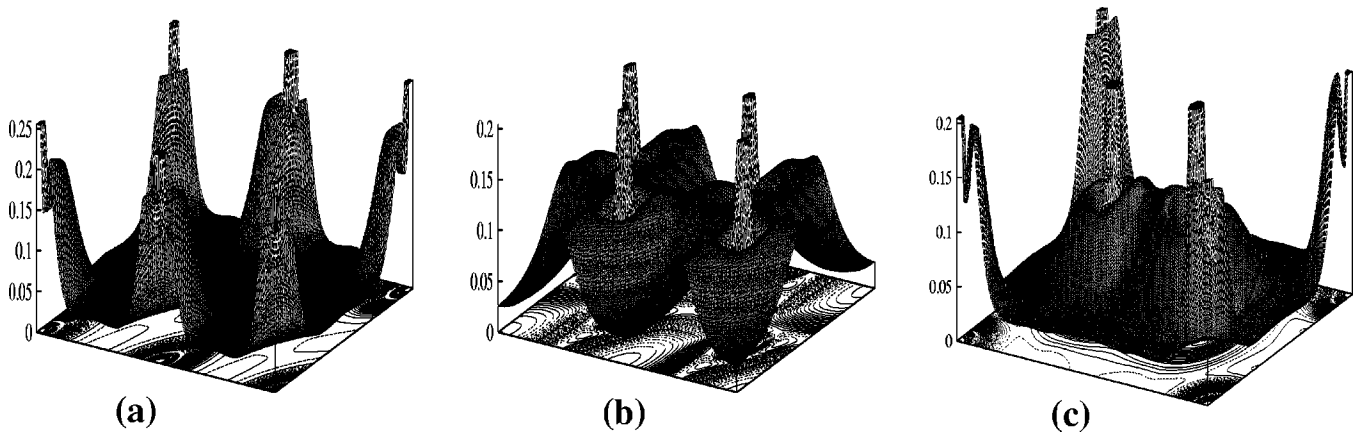

FIG. 5. Valence electron charge density plot for TiB_2 in (a) the (0001) plane where the Ti-Ti bonding is present, (b) the (0002) plane where the B-B bonding is present, and (c) the $(10\bar{1}0)$ plane where the Ti-Ti, B-B, and Ti-B bondings are present where Ti atoms are in the corner. In all plots 50 contours are drawn between 0 to 0.25 electrons/a.u.^{3}.

finite covalent interaction between Ti and B in TiB_2 and this covalent interaction is not as strong as that between boron atoms in TiB_2. The present observation of weaker covalent interaction between TM-B compared with between B-B is inconsistent with the conclusion arrived from the thermal expansion coefficient measurement.[57]

For all the diborides there is a considerable electron drift towards the boron atoms and this gives rise to a substantial ionic contribution to the bonding. The magnitude of this electron donation decreases from ScB_2 to FeB_2 in the $3d$ series. The present observation of finite charge transfer from TM to B in early $3d$ TMB_2 compounds is in agreement with the conclusion recently arrived from the discrete-variational $X\alpha$ method.[58] To analyze the variation in the bonding behavior of TMB_2 compounds by band filling we have given the charge density distribution for $3d$ transition metal diborides in Fig. 6. From this figure one can see that the bonding between Sc-B is weaker compared with that between TM-B in other TMB_2 compounds. There is a negligible charge density distribution between Sc and B in ScB_2 indicating that the Sc-B bond is not dominantly covalent in nature. When considering large electronegativity difference between Sc and B we conclude that there is an ionic bonding between Sc and B. The bonding between boron atoms in all these compounds is of covalent nature and does not change significantly along this series. This is in agreement with the experimental obser-

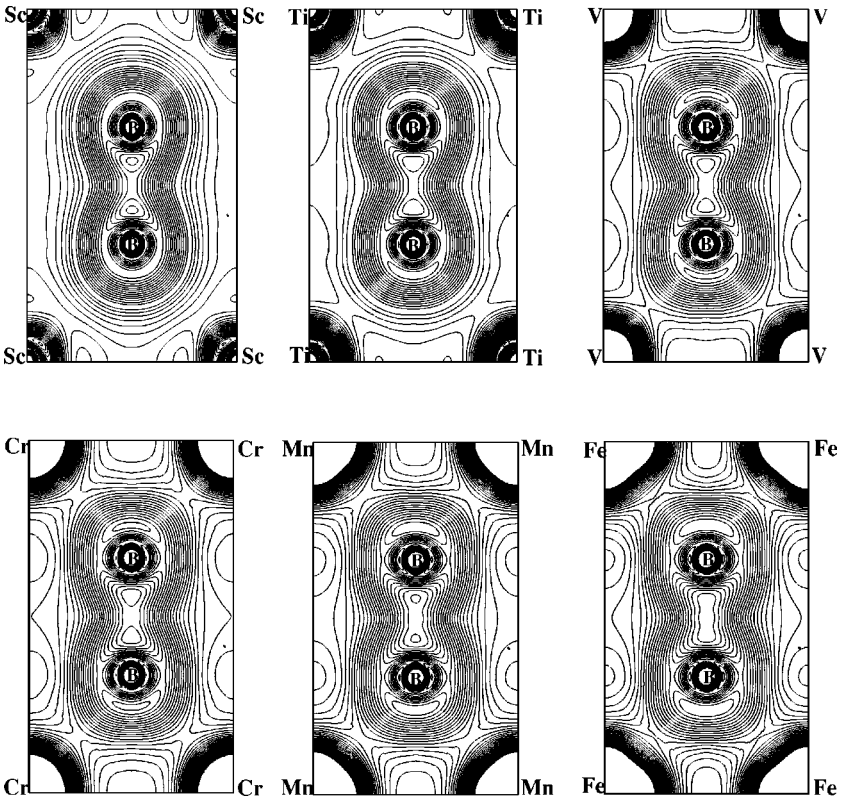

FIG. 6. Valence electron charge density plot for ScB_2, TiB_2, VB_2, CrB_2, MnB_2, and FeB_2 in the $(10\bar{1}0)$ plane with 50 contours are drawn between 0 to 0.25 electrons/a.u.^{3}. In the case of CrB_2 and MnB_2, the charge density is calculated from the spin-polarized calculation.

vation of very little change in the bond strength within the boron layer by the introduction of larger metal atoms.[57] The covalent interaction between transition metals systematically increases with increase of *d*-band filling. It should also be noted that the TM-TM distance decreases from ScB_2 down to FeB_2 progressively, which facilitates greater *p*-*d* and *d*-*d* interaction. Our calculations show that the bonding behavior in TiB_2 is the combination of ionic, covalent, and metallic nature. Even though TiB_2 has high melting point and large cohesive energy, its bonding behavior is not different from the other compounds. So, the distinguished nature of ground state behavior in TiB_2 among $3d$ TMB_2 compounds is originating from the band filling effect, i.e., the falling of E_F at the pseudogap. In the case of CrB_2 and MnB_2, we found covalent interaction between transition metal and boron. This is the reason why our calculated magnetic moments are much smaller than that of the corresponding transition metals. For FeB_2, the calculation shows strong covalent interaction between Fe and B. As a result, the magnetic moment is completely quenched in this material.

VI. COHESIVE PROPERTIES

It is to be noted that as the *d* electron number increases, the bonding states get filled accompanied by a decrease in the equilibrium volume. The equilibrium volume is the minimum when the band is half filled and beyond this, it increases with the filling of the valence band. This trend can be seen from the equilibrium volumes given in Table I. The cohesive energy of a material is a fundamental property which has long been the subject of theoretical and computational approaches. The chemical bonding is a mixture between covalent, ionic, and metallic bonding and therefore the cohesive energy cannot be determined reliably from simple models. Thus, first principles calculations based on density functional theory (DFT) have become a useful tool to determine the cohesive energy of the solids. In this connection, the cohesive energy of TMB_2 is calculated by using the expression

$$E_{\mathrm{coh}}^{AB_2}=[E_{\mathrm{atom}}^{A}+2E_{\mathrm{atom}}^{B}]-E_{\mathrm{total}}^{AB_2}, \tag{1}$$

where $E_{\mathrm{total}}^{AB_2}$ refers to the total energy of the compound at equilibrium lattice constants and E_{atom}^{A} and E_{atom}^{B} are the atomic energies of the pure constituents calculated semirelativistically. To determine the heat of formation, we have first calculated the total energies of TM elements and B corresponding to their respective equilibrium lattice parameters. At zero temperature, there is no entropy contribution to the free energy, therefore the free energy of formation, or the heat of formation (ΔH) can be obtained from the following relation:

$$\Delta H^{AB_2}=E_{\mathrm{total}}^{AB_2}-[E_{\mathrm{solid}}^{A}+2E_{\mathrm{solid}}^{B}], \tag{2}$$

where $E_{\mathrm{total}}^{AB_2}$ refers to the total energy of TMB_2 at equilibrium lattice constants and E_{solid}^{A} and E_{solid}^{B} are total energy of the pure elemental constituents.

TABLE II. Calculated (pre.) and experimental (expt.) bulk modulus (B_0 in Mbar), its pressure derivative (B_0'), heat of formation ($-\Delta H$ in KJ mol^{-1}), and cohesive energy (E_{coh} in Ry $atom^{-1}$) for TMB_2 compounds.

Compound	B_0 (pre.)	B_0'	B_0 (expt.)	$-\Delta H$ (pre.)	$-\Delta H$ (expt.)	E_{coh} (pre.)
ScB_2	1.91	1.85	-	231.52	307	1.17
TiB_2	2.13	2.1	2.02	308.38	328[a]	1.32
VB_2	1.75	1.67	-	208.14	206[a]	1.01
CrB_2	1.56	1.68	-	181.93	133[a]	0.98
MnB_2	2.1	1.65	-	140.04	120[a]	0.88
FeB_2	2.3	1.69	-	113.71	94.14[a]	0.79
YB_2	1.41	2.05	-	101.68	105[a]	0.88
ZrB_2	1.95	1.94	2.15	296.81	322.59[b]	1.25
NbB_2	1.01	1.67	-	192.73	197[a]	0.94
MoB_2	1.6	1.71	-	131.61	-	0.83
HfB_2	2.16	1.35	2.12	244.20	335.98[b]	1.21
TaB_2	1.82	1.78	-	179.15	209.20[b]	0.98

[a]Reference 19.
[b]Reference 77.

The cohesive properties of $3d$ metal carbides and nitrides[59] indicate that the number of valence electrons per atom n_e is a useful variable in correlating properties related to the cohesive energy of compounds which have a similar type of chemical bonding. So, for the present study, we use $n_e(n_{\mathrm{TM}}+2n_{\mathrm{B}})/3$, where n_{TM} and n_{B} are the number of valence electrons for transition metal and boron, respectively. The calculated values of the cohesive energies and heat of formation of all systems are given in Table II. The systematic errors in total energy due to the use of ASA are canceled significantly, leading to a reasonably accurate formation energy. The heat of formation energies calculated for these compounds are in good agreement with the experimental values.[60,61] In order to understand the role of band filling on the stability of these materials, the n_e vs ΔH is shown in Fig. 7 and also a comparison is made with experimental ΔH in this figure. It is interesting to note that the present theoretical values coincide with experimentally reported values for VB_2 and early transition metal diborides. On the other hand, the experimental values are higher than the theoretical values for the diborides whose n_e is greater than that of VB_2. This is partly due to the noninclusion of magnetic correlation effects in our calculation. Further, the experimental calorimetric measurements were made[19] at high temperature and our calculated ΔH value is applicable only for low temperatures. In the case of $4d$ and $5d$ series the calculated values are coinciding very well with experimental values. We also note that the $3d$ compounds usually show the most exothermic enthalpies of formation and that the values tend to decrease systematically as we go from $3d$ to $4d$ to $5d$ metals. Further, the ΔH is higher for TiB_2, ZrB_2, and HfB_2 in the $3d$, $4d$, and $5d$ series, respectively, which is related to the unique properties such as high hardness, high melting point with maximum corrosion resistance among the compounds in the series. The origin of the unique properties of these com-

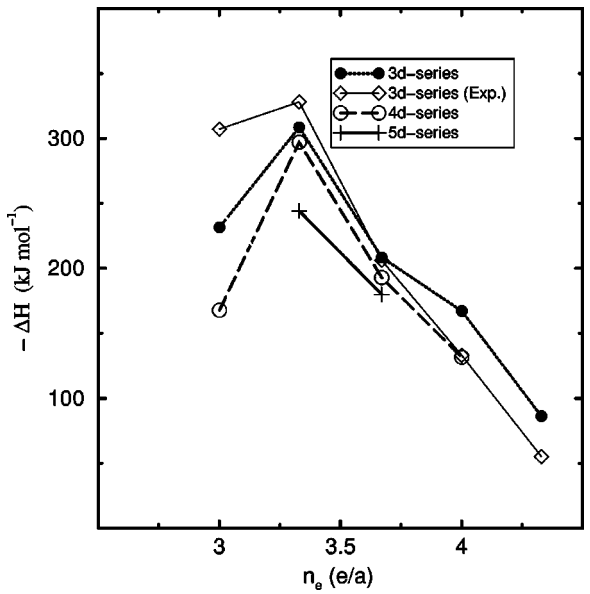

FIG. 7. Number of electrons per atom (n_e) vs heat of formation (ΔH kJ mol^{-1}) in TMB_2 compounds.

pounds among the TMB_2 compounds is due to band-filling effect which is discussed in detail below.

The E_F of TiB_2, ZrB_2 and HfB_2 falls near the minimum in the DOS curve in Figs. 2 and 3. This means that, all the bonding states are filled and the antibonding states are empty for the electron per atom $n_e=3.33$. As a result, the cohesive-related properties such as the melting temperature and the enthalpy of formation will be higher as shown in Fig. 7. In a rigid-band picture, we would start to populate antibonding states when n_e is increased above $3.33e/a$ and consequently the cohesive-related properties will be reduced. When n_e decreases below $3.33e/a$ one cannot make full use of all the bonding states and that also leads to a reduction in the cohesion. We observe that the filling up of bonding orbitals leads to a positive slope and the filling up of antibonding orbitals leads to a negative slope as shown in Fig. 7. Although a rigid-band approach would be too crude to give direct quantitative estimates of ΔH, for example, it is expected to give the trends as a function of n_e. From Fig. 7, it is clear that the rigid band picture works well in these materials.

A. Bulk modulus and its pressure derivative

Experimental bulk modulus values are not available for most of these compounds and this is the first report on the values of B_0 for those compounds. An universal relationship between the binding energies and distances between atoms has been discovered for bimetallic adhesion,[62] chemisorption on metals,[63] and metallic cohesion.[64] Later Vinet *et al.*[65] proposed a universal model of the equation of state (UEOS) for all classes of solids in compression, which is claimed to be superior to that of the Birch-Murnaghan EOS.[66] If we define x as $(V/V_0)^{1/3}$ and $H(x)$ as $x^2P(x)/3(1-x)$, the $\ln[H(x)]$ vs $(1-x)$ curve should be nearly linear according to their theory; i.e., $\ln[H(x)]=\ln B_0+\eta(1-x)$ and the EOS at a given temperature can be expressed as

$$P=3B_0\frac{(1-x)}{x^2}e^{\eta(1-x)}, \tag{3}$$

where $\eta=\frac{3}{2}(B_0'-1)$ is the slope of the curve. It is related to the pressure derivative of the bulk modulus B_0'. We have calculated the values of $\ln[H(x)]$ and $(1-x)$ using the pressure-volume (P-V) data and made the least-squares fit in a manner similar to what we have made earlier.[31,67,68] In the case of TMB_2, the bonding nature can be regarded as a combination of metallic, covalent, and partly ionic bonding.[10] The UEOS is suitable for describing mixed bonding systems.[65] To determine the bulk modulus, we have carried out self-consistent calculations for six different volumes within the volume range $V/V_0=1.15$ to 0.85 which is 15% around the experimental equilibrium volume. The calculated bulk modulus is given in Table II.

For materials at the beginning of a transition series, the bonding orbitals begin to fill, leading to increase in cohesion and hence to a decrease in the atomic volume. This decreased atomic volume and increased compression of *s* orbitals lead to an increase in the bulk modulus. These effects are all maximized near the middle of the transition series,[69] when all the bonding orbitals are filled, and then the trend is reversed when the antibonding orbitals begin to be filled. We also identify the same trend in TMB_2 compounds currently under consideration. The calculated bulk modulus values are compared with the available experimental values in Table II. From this table, it can be seen that our calculated values are in good agreement with the experimental values. The B_0 value is found to be maximum for $5d$ HfB_2, followed by $3d$ TiB_2 and $4d$ series diboride ZrB_2. This trend is in agreement with the reported experimental values. Generally, the compounds with high melting temperature T_m are expected to have high B_0. The melting temperatures of HfB_2, ZrB_2, and TiB_2 are 3523, 3313, and 3253 K, respectively. However, the B_0 values are higher for TiB_2 than for ZrB_2. The T_m is defined by both bulk modulus and the shear modulus.[70] So, the observation of no systematic trend between B_0 and T_m indicates that the shear contribution varies significantly among these compounds. To the best of our knowledge, B_0 values are available only for IVB compounds. Neither the theoretical nor the experimental values of B_0 are available for the rest of the compounds under study. It should be noted that the B_0 values of the present calculation are in good agreement with the available experimental values. However, the calculated B_0 value of TiB_2 by Tian and Wang[10] in the earlier theoretical calculation is an overestimate when compared with the experimental as well as our theoretical work. This variation in the B_0 values between ours and the Wang calculation is due to the *k* point optimization. So, we believe that our calculated values are more reliable for other compounds also.

The pressure derivative of bulk modulus at zero pressure B_0' is a parameter of great physical significance in high pressure physics. It is related to a few other important thermophysical properties (like phase transitions, interphase energy, adsorption energy, etc.).[71] Generally, the variation along the period is one of gradual increase, roughly until the middle of

TABLE III. The calculated density of states at the Fermi level [$N(E_F)$ in states Ry^{-1} f.u.$^{-1}$], electronic specific heat coefficient (γ in mJ mol^{-1} K^{-2}), and electron phonon coupling constant (λ) for TMB_2 compounds. The results obtained from the spin-polarized calculations are represented by (spin).

Compound	$N(E_F)$	$\gamma_{present}$	γ_{exp}	γ_{theo}	λ
ScB_2	11.99	2.08	2.2	2.48	0.058
TiB_2	4.27	0.74	1.08	0.38	0.459
VB_2	15.86	2.48	4.84	3.62	0.952
CrB_2	34.88	6.05	13.6	5.84	1.247
CrB_2(spin)	37.89	6.57	-	1.070	-
MnB_2	108.94	18.89	-	8.09	-
MnB_2(spin)	20.18	3.51	4.45	-	0.26
FeB_2	37.28	6.46	-	-	-
YB_2	11.68	2.03	-	2.38	-
ZrB_2	3.84	0.67	-	0.36	-
NbB_2	13.95	2.42	2.33	2.44	-
MoB_2	20.01	3.47	3.58	2.76	0.032
HfB_2	3.688	0.64	-	0.34	-
TaB_2	12.92	2.24	1.7	2.37	-

the period, followed by a drop for the remaining elements. The increasing trend can be attributed to the increasing level of filling in the bonding *d* level which reaches a saturation at the middle of the period. The same behavior is not valid for the entire *d*-block elements. The B_0' is directly related to the electron density in the *d*-series elements, the element with lowest B_0' will have high electron density. It is valid for only $3d$-elements and not for $4d$ and $5d$ series in the TMB_2 compounds. We compare the B_0' values of the TMB_2 compounds with that of constituent transition element. It is found that the B_0' of these compounds is half that of the constituent transition element. This indicates the strong interlayer and intralayer chemical bonding in TMB_2 compounds.

B. Electronic specific heat coefficient

The linear term in the specific heat at low temperatures γ is proportional to the $N(E_F)$. Values of γ for transition metal mono- and diborides are measured by earlier works.[10,15] In Table III, we have compared the electronic specific-heat coefficient γ obtained from the present study with the available theoretically calculated values and experimental values. The theoretical values are calculated directly from the free electron approximation, $\gamma=(\pi^2/3)N(E_F)k_B^2$, using the calculated density of states at the Fermi energy. The calculated γ values will always be higher than the experimental values since the electron–phonon enhancement effect is not taken into account in our calculations. The present theoretical values are found to be in agreement with the other theoretically calculated values as given in Table III.

The calculated $N(E_F)$ values are very sensitive to the number of *k* points used in the calculations. So, the discrepancy between the present results with the earlier reported[12] theoretical values is partly due to the *k* point effect. As mentioned above, the calculated values usually underestimate with experimental values, because the electron–phonon enhancement factor is not included in the theoretical calculations. But, surprisingly, our calculated values overestimate the γ values in the case of CrB_2, MnB_2, and FeB_2 in the $3d$ series, NbB_2 in the $4d$ series, and TaB_2 in the $5d$ series (earlier works also find this variation). At least, the discrepancy in the $3d$ transition metal diborides can be accounted for by the magnetic correlation effect in these compounds. For example, the γ value is very large compared with the experimental γ value for MnB_2 because of the higher $N(E_F)$. So the spin polarized calculation is made for this compound and it reduces the γ values considerably. Among these diborides, HfB_2 has small γ value and the VIB compounds have high γ value. We have also estimated the electron-phonon enhancement factor λ for these materials using the experimentally reported γ values by the relation $\gamma_{exp}=\gamma_{th}(1+\lambda)$, where γ_{exp} and γ_{th} refer to the experimental and theoretical values of electronic specific heat coefficients, respectively. In the case of TaB_2 and NbB_2, we have obtained γ values larger than the experimentally reported values. So, we have not given the λ values for these compounds in Table III. In order to clarify the theoretically obtained large γ in these compounds, more accurate electronic specific heat coefficient measurements at low temperatures are needed. In the other compounds, the calculated λ values are found to be much smaller than those of the superconducting materials. These TMB_2 compounds do not obey the Matthias rule,[72] which relates the optimal electron concentration for superconductivity (5 and 7 electrons per atom), whereas the electron per atom ratio for these compounds is less than 5. This may be the possible reason for the low λ values and the nonobservation of superconductivity ($T_c<1$ K) in these compounds.[73] The present observation of large γ values in some of the TMB_2 compounds compared with the experimental study is due to the nonreliable experimental γ value or the failure of LDA.

VII. CHEMICAL STABILITY

It is well known that the chemical stability is associated with melting point. Compounds with high melting points generally have high chemical stability. It is interesting to note that the melting temperature of the elements Sc to Cr in the periodic table increases linearly. On the other hand, the melting temperature of these elements is found to decrease with the addition of boron, where the T_m decreases from TiB_2 to CrB_2 in the $3d$ series, ZrB_2 to MoB_2 in the $4d$ series, and HfB_2 to TaB_2 in the case of $5d$ series. This discrepancy can be explained as follows: In the case of transition metals the number of bonding states increases with the increase of *d* electron number and gets maximum in the middle of the series. Since the filling of bonding states enhances the bond strength, the T_m increases while going from Sc to Cr. On the other hand, all the bonding states get filled in IVB-TMB_2 compound itself due to the presence of pseudogap at E_F. So, the increase in *d* electrons when going from TiB_2 to FeB_2 fills the antibonding/nonbonding states. As the filling of antibonding/nonbonding is less favorable for

TABLE IV. The width of the valence band (W_v in Ry), width of the bonding states (W_p in Ry), W_v/W_p, and melting point (T_m in K) for the TMB_2 compounds.

Compound	W_v	W_p	W_v/W_p (pre.)	W_v/W_p (Ref. 12)	T_m
ScB_2	0.76	0.88	0.87	0.90	2523
TiB_2	0.90	0.89	1.01	0.99	3253–3498
VB_2	0.96	0.88	1.10	1.03	2673–3020
CrB_2	1.05	0.95	1.11	1.12	2473
MnB_2	1.03	0.95	1.09	1.13	2261
FeB_2	1.01	0.93	1.10	-	-
YB_2	0.75	0.88	0.86	0.76	2373
ZrB_2	0.93	0.88	1.05	0.99	3313–3518
NbB_2	1.18	0.85	1.17	1.02	3173–3309
MoB_2	1.08	0.88	1.23	1.14	2373–2648
HfB_2	0.98	0.93	1.05	1.02	3373–3653
TaB_2	1.10	0.98	1.12	1.14	3310–3473

chemical stability, T_m decreases with increase of d electron number. The lower $N(E_F)$ is often related with higher stability and higher melting point.[35] This can be understood as follows: If a material has large $N(E_F)$, it means that large density of electrons is present in the highest occupied level, i.e., in the vicinity of the Fermi level. It is not a favorable condition for stability since the one electron eigenvalue sum increases and hence lattice instability will arise easily resulting in lower melting point. On the other hand, if the $N(E_F)$ value is small, it means that the electrons participate in bonding and get localized. As a result, the stability of the material will be larger and will possess higher melting point. The present observation indicates that the electrons at the Fermi level mainly decide the melting behavior of solids.

We have analyzed the chemical stability of these compounds using the band filling of the bonding states as follows: As the rigid-band model describes the electronic structure of the diborides rather well, the band filling can naturally be regarded as being responsible for the variations of their electronic structure and related properties. We define W_v, the energy difference from bottom of the valence band to the Fermi level and W_p, the energy width from the bottom of the valence band to the pseudogap. Since W_v represents the width of the occupied states and W_p represents the bonding states, W_v/W_p can be used to describe the occupied portion of the bonding states. Here, the W_p is found to be almost constant, while the W_v alone varies for different compounds depending upon the number of valence electrons. The calculated values of W_v/W_p for TMB_2 compounds are listed in Table IV along with those reported in Ref. 12. From this table it should be noted that ScB_2 has 9 valence electrons and its bonding states are not fully filled ($W_v/W_p<1$). In the case of TiB_2, W_v/W_p is almost equal to unity. This indicates that all the bonding states are filled and all the antibonding states are empty. From CrB_2 to FeB_2 the W_v/W_p factor systematically increases and also becomes greater than unity (see Table IV). This indicates that the bonding states are already filled and the antibonding/nonbonding states get occupied when going from CrB_2 to FeB_2. So the chemical stability is in the following order for the $3d$ transition metal diborides: $TiB_2>VB_2>CrB_2>MnB_2>FeB_2$, in the $4d$ series $ZrB_2>NbB_2>MoB_2$, and in the $5d$ series $HfB_2>TaB_2$. For comparison we have given the W_v/W_p obtained by Wang *et al.* in Table IV along with our results. It should be noted that there is significant difference between our results and those reported in Ref. 12. Since we have used k-point optimization in our calculations we believe that our results are quantitatively closer to reality. Even though there is quantitative difference between the present result and Ref. 12, from Table IV one can see that qualitatively both results are consistent with each other.

The ScB_2 and YB_2 compounds need more electrons into the band to increase the stability of these compounds. In the $3d$-transition metal diboride series TiB_2 has enough space to accommodate its 10 valence electrons. So it is expected to be the most stable compound in this series. In the case of isoelectronic compounds along the group where the number of valence electrons remains the same, the chemical stability is in the following sequence: $TiB_2<ZrB_2<HfB_2$ in the fourth group and $VB_2<NbB_2<TaB_2$ in the fifth group. The remaining compounds also follow this sequence. A similar trend is observed in the other theoretical[12] as well as experimental works. The large chemical stability in the $5d$ series transition metal diborides over the corresponding $3d$ or $4d$ transition metal diborides is due to the enhancement in the covalent hybridization between the transition metal and boron, because when we go down the periodic table in a particular group, one can expect the delocalization of valence band due to the screening effect. Hence, compared to Ti, the outermost electrons in Hf are much delocalized. As a result of this, the valence electrons for Hf will have strong covalent interaction with the boron compared with that of Ti. This hybridization effect will separate the bonding states from the antibonding/nonbonding states which leads to low $N(E_F)$. This may be the possible explanation for the high melting point for HfB_2 over TiB_2. From the above analysis, the band structure calculations were found to explain the chemical stability of these TMB_2 systems successfully.

VIII. THE MAGNETIC PROPERTIES

CrB_2 has a complicated helicoidal magnetic structure, as resolved by neutron diffraction measurements.[74] But for simplicity, we have assumed the ferromagnetic ordering in our calculation. Early magnetization and susceptibility measurements yielded rather surprising results that MnB_2 is a simple ferromagnet with a small saturated moment of 0.25 μ_B/Mn atom[49] and 0.19 μ_B/Mn atom[75] and an ordering temperature of 157 ± 3 K[49] and 143 K.[75] FeB_2 is metastable in the Fe-B system, and its magnetic properties are not known. However, the possible existence of a magnetic transition in this phase cannot be ruled out in view of the ferromagnetic transitions in the stable iron boride phases Fe_2B and FeB.[22,76]

The spin polarized calculations are performed for CrB_2, MnB_2, and FeB_2. Filling up of the d band moves the Fermi energy into a region of high DOS where both CrB_2 and MnB_2 fulfill the Stoner criterion. FeB_2 also has high DOS at

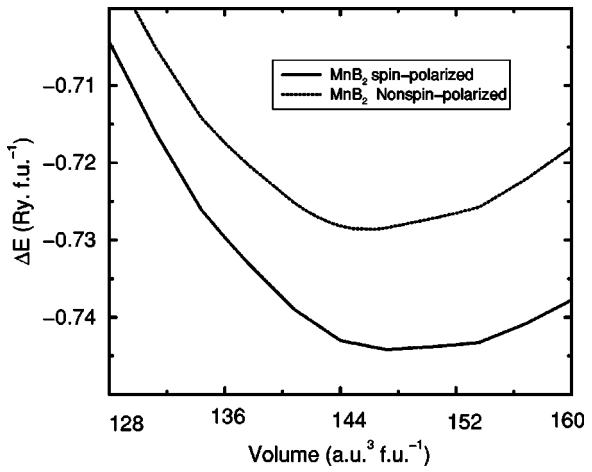

FIG. 8. The total energy vs unit cell volume curves for MnB_2 from the spin-polarized and non-spin-polarized calculation where $\Delta E = E + 2412$.

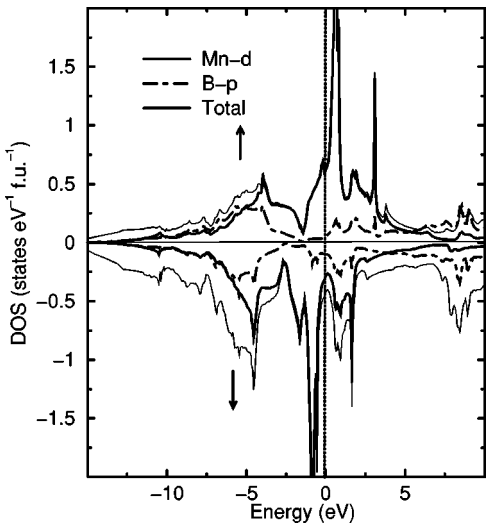

FIG. 9. The spin projected DOS for MnB_2 in the ferromagnetic phase.

the Fermi level, but we do not observe spontaneous spin polarization in this case. As mentioned above, our charge density analysis shows that there is a strong covalent bonding between Fe and B in FeB_2 compared to the other transition metal compounds considered here. So, the observation of nonmagnetic behavior in FeB_2 is due to the participation of electrons in the chemical bonding instead of magnetism. The variation of total energy with volume for MnB_2 with and without spin polarization are given in Fig. 8. From this curve, it is clear that a large gain in total energy is observed by the inclusion of spin polarization in our calculation. So, our calculation predicts that the ferromagnetic state is energetically more favorable than the nonmagnetic state in MnB_2. It is consistent with the experimental studies in the sense that the magnetization and susceptibility studies suggest[49,75] an itinerant band ferromagnetic behavior in MnB_2. However, our calculation yields the magnetic moment of 1.6 μ_B/Mn, and this is much higher than the experimentally observed value. Very recent theoretical studies[21] on MnB_2 suggest that spin canting structure could be responsible for the small ferromagnetic component found in the experiment. The equilibrium cell volume of the spin-polarized case is 155.632 a.u.^{3}, 149.345 a.u.^{3} and that of the nonspin-polarized case is 154.763 a.u.^{3}, 149.325 a.u.^{3} for CrB_2 and MnB_2, respectively. The enhancement in the equilibrium volume by the inclusion of spin polarization in our calculation is due to magnetovolume effect.

The calculated total, site, and spin projected DOS for MnB_2 obtained from the spin polarized calculation are shown in Fig. 9. It should be noted that the E_F falls on a sharp peak (Fig. 2) in the nonspin polarized case of MnB_2 (see Fig. 2). On the other hand, the spin polarization splits the Mn-d DOS in such a way that the E_F lies in a valley region in the total DOS as shown in Fig. 9. As a consequence of this, we have obtained a small value of γ compared with that of the nonspin-polarized case which is closer to the experimentally reported value (Table III). In the case of CrB_2, we observed a very small magnetic moment of 0.32 μ_B/Cr. Hence, the DOS does not change significantly when going from the nonspin-polarized case to the spin-polarized case. As a result, the E_F is present in the shoulder of DOS peak which possesses a dominant nonbonding Cr 3d character. This is not a favorable condition for stability. This may be the possible reason for the stabilization of complex helicoidal magnetic structure in CrB_2. Our calculated magnetic moment of CrB_2 is found to be close to the experimentally measured[74] magnetic moment of 0.5 ± 0.1 μ_B/Cr. The gain in total energy by spin polarization obviously reflects the formation energy and hence the recalculated formation energy for MnB_2 and CrB_2 are -150.43 and -184.24 KJ mol^{-1}, respectively. The previous calculations on mono-[14] and semiboride[20] of Fe show a reduction in the magnetic moment on boron addition to Fe with the magnetic moment values of 1.91 μ_B/Fe for Fe_2B and 1.12 μ_B/Fe for FeB. From our calculations we found that further addition of boron in FeB is found to suppress the magnetic moment in the FeB_2 case. But the opposite trend was observed in the case of MnB_2 where Khmelevsky and Mohn[21] found that the addition of B in the Mn_2B matrix increases the magnetic moment up to MnB. In the case of MnB_2, we found that the magnetic moment is exactly the same as in Mn_2B, indicating an increase in the magnetic moment on addition of B up to a certain range after which further addition of boron reduces the magnetic moment. In the case of CrB and Cr_2B, no magnetic moment is observed. But in the CrB_2 case, we find a small amount of magnetic moment.

IX. SUMMARY AND CONCLUSION

We have performed first-principles local density functional electronic structure calculation for the 12 TMB_2 compounds using the TB-LMTO-ASA method. The calculated lattice constants are found to be in very good agreement with experimental results. These TMB_2 compounds are not exactly layered compounds because of the d-d interaction among the TM and the interaction of TM-d electrons with the p electrons of the B atom present in these phases. The

cohesive energy, heat of formation, and bulk modulus for most of these compounds are calculated for the first time. We list the important conclusions arrived from our calculations.

(1) We successfully explained the chemical bonding behavior of AlB_2-type TMB_2 compounds from our DOS and charge density analysis. The covalent nature of bonding in these compounds systematically increases with increase of n_e along the series. These compounds possess mixed bonding nature such as strong covalent bonding between boron, metallic, and covalent bonding between transition metals, and ionic and covalent bonding between TM and B.

(2) The calculated cohesive properties such as heat of formation are found to be in good agreement with the experimental values and the change in trend along the series is explained via the band filling of the bonding state analysis.

(3) The calculated electron phonon enhancement factor λ for TMB_2 compounds is very small compared with the superconducting compounds.

(4) From the DOS histogram, we found that pseudogap is a common feature for all these compounds. The most popular belief for the origin of pseudogap is that it arises due to the p-d σ bonding between nonmetal and transition metal nonmetal atoms in most of the intermetallic compounds.[78] But, in the present systems, the common origin for the creation of pseudogap in all these materials is due to strong covalent bonding between boron atoms.

(5) Calculated bulk modulus and its pressure derivatives are compared with available experimental and other theoretical values. The calculated bulk modulus values are found to be in good agreement with experimental values.

(6) The electron band structure total energy studies show that the cohesive-related properties show a maximum in bond strength for TiB_2 in the $3d$ TMB_2 compounds and this is due to the maximum filling of bonding states.

(7) We found finite magnetic moment in MnB_2 and CrB_2 from our spin-polarized calculations. Due to strong covalent bonding between Fe and B, our calculation predicts a nonmagnetic behavior in FeB_2.

ACKNOWLEDGMENTS

The first author (P.V.) gratefully acknowledges the financial support from DST, India and R. Vidya and R. Rita for their encouragement at several stages of this work. P.R. wishes to thank P.A. Korzhavyi and L. Offernes for useful discussions.

*Electronic address: ravi@kjemi.uio.no

[1] E. A. Knyshev, V. M. Novgorodtsev, U. S. Plyshevski, V. A. Kobyakov, Z. G. Stepanova, V. V. Svistunov, and A. R. Beketov, J. Less-Common Met. **47**, 273 (1976).
[2] E. P. Wohlfarth, J. Magn. Magn. Mater. **7**, 113 (1978).
[3] W. Gordon and S. B. Soffer, J. Phys. Chem. Solids **36**, 627 (1975).
[4] B. Loundquist, H. Myers, and R. Westin, Philos. Mag. **33**, 1187 (1960).
[5] V. A. Neronov, M. A. Korchagin, V. V. Aleksandrov, and S. N. Gusenko, J. Less-Common Met. **82**, 125 (1981).
[6] V. S. Sinelnikova, V. N. Gurin, A. N. Pilyankevich, L. V. Strashinskaya, and M. M. Korsukova, J. Less-Common Met. **47**, 265 (1976).
[7] S. Otani and Y. Ishizawa, J. Cryst. Growth **140**, 451 (1994).
[8] T. Lundstrom, B. Lonnberg, and I. Westman, J. Less-Common Met. **96**, 229 (1984).
[9] B. Champagne, S. Dallaire, and A. Adnot, J. Less-Common Met. **98**, L21 (1983).
[10] D. C. Tian and X. B. Wang, J. Phys.: Condens. Matter **4**, 8765 (1992).
[11] R. R. Atri, K. S. Ravichandran, and S. K. Jha, Mater. Sci. Eng., A **271**, 150 (1999).
[12] X. B. Wang, D. C. Tian, and L. Wang, J. Phys.: Condens. Matter **6**, 10 185 (1994).
[13] J. K. Burdett, E. Lanadell, and G. J. Miller, J. Am. Chem. Soc. **108**, 6561 (1986).
[14] P. Mohn and D. G. Pettifor, J. Phys. C **21**, 2829 (1988).
[15] J. Castaing, R. Caudron, G. Toupance, and P. Costa, Solid State Commun. **7**, 1453 (1969).
[16] D. E. Wiley, W. R. Manning, and O. Hunter, J. Less-Common Met. **8**, 149 (1969).
[17] P. S. Spoor, J. D. Maynard, M. J. Pan, D. J. Green, J. R. Hellmann, and T. Tanaka, Appl. Phys. Lett. **70**, 9159 (1997).
[18] S. I. Wright, J. Appl. Crystallogr. **27**, 794 (1994).
[19] L. Topor and O. J. Kleppa, J. Chem. Thermodyn. **17**, 1003 (1985).
[20] P. Mohn, J. Phys. C **21**, 2841 (1988).
[21] S. Khmelevskyi and P. Mohn, Solid State Commun. **113**, 509 (2000).
[22] M. C. Cadeville and A. J. P. Meyer, C. R. Hebd. Seances Acad. Sci. **255**, 3391 (1962).
[23] S. H. Liu, L. Kopp, W. B. England, and H. W. Myron, Phys. Rev. B **11**, 3465 (1975).
[24] H. Ihara, M. Hirabayashi, and H. Nakagawa, Phys. Rev. B **16**, 726 (1977).
[25] P. G. Perkins and A. V. J. Sweeney, J. Less-Common Met. **47**, 165 (1976).
[26] O. K. Andersen, Phys. Rev. B **12**, 3060 (1975).
[27] H. L. Skriver, *The LMTO Method* (Springer, Heidelberg, 1984).
[28] O. K. Andersen and O. Jepsen, Phys. Rev. Lett. **53**, 2571 (1984).
[29] O. K. Andersen, in *Methods of Electronic Structure Calculations*, edited by O. K. Andersen, V. Kumar, and A. Mookerjee (World Scientific, Singapore, 1994).
[30] U. von Barth and L. Hedin, J. Phys. C **5**, 1629 (1972).
[31] P. Ravindran and R. Asokamani, Phys. Rev. B **50**, 668 (1994).
[32] S. Otani, M. M. Korsukova, and T. Mitsuhashi, J. Cryst. Growth **186**, 582 (1998).
[33] M. L. Cohen, Phys. Rep. **110**, 293 (1983).
[34] A. R. Williams, J. Kubler, and C. D. Gelatt, Phys. Rev. B **19**, 6094 (1979).
[35] J. H. Xu and A. J. Freeman, Phys. Rev. B **41**, 12 553 (1990).
[36] A. Pasturel, C. Colinet, and P. Hicter, Physica B & C **132**, 177 (1985).
[37] J. C. Phillips, Phys. Rev. B **47**, 2522 (1992).
[38] O. Jepsen, O. K. Andersen, and A. R. Mackintosh, Phys. Rev. B **12**, 3084 (1975).

[39] K. Lie, R. Brydson, and H. Davock, Phys. Rev. B **59**, 5361 (1999).
[40] E. Dempsey, Philos. Mag. **8**, 285 (1963).
[41] H. J. Juretschke and R. Stinitz, J. Phys. Chem. Solids **4**, 118 (1958).
[42] G. V. Samsonov, Yu. M. Goryachev, and B. A. Kovenskaya, J. Less-Common Met. **47**, 147 (1976).
[43] W. N. Lipscomb and D. Britton, J. Chem. Phys. **33**, 275 (1960).
[44] K. E. Spear, J. Less-Common Met. **47**, 195 (1976).
[45] B. Post, F. W. Glaser, and D. Moskowitz, Acta Metall. **2**, 20 (1954).
[46] J. Piper, J. Phys. Chem. Solids **27**, 1907 (1966).
[47] Y. S. Tyan, L. E. Toth, and Y. A. Chang, J. Phys. Chem. Solids **30**, 785 (1969).
[48] R. Kiessling, Acta Chem. Scand. **4**, 209 (1958).
[49] M. C. Cadeville, J. Chem. Solids **27**, 667 (1966).
[50] L. Pauling, Proc. R. Soc. London, Ser. A **196**, 343 (1949).
[51] H. C. Longuet-Higgins and M. Roberts, Proc. R. Soc. London, Ser. A **224**, 336 (1954).
[52] R. W. Johnson and A. H. Daane, J. Chem. Phys. **38**, 425 (1963).
[53] G. V. Samsonov and B. A. Kovenskaya, in *Boron and Refractory Borides*, edited by V. I. Matkovich (Springer-Verlag, Berlin, 1977), pp. 5,19.
[54] B. Post, in *Boron, Metallo-Boron Compounds and Boranes*, edited by R. M. Adams (Interscience Publishers, New York, 1964), pp. 301,313.
[55] V. M. Anishchik and N. N. Dorozhkin, Phys. Status Solidi B **160**, 173 (1990).
[56] D. R. Armstrong, Theor. Chim. Acta **64**, 137 (1983).
[57] B. Lönnberg, J. Less-Common Met. **141**, 145 (1988).
[58] M. Mizuno, I. Tanaka, and H. Adachi, Phys. Rev. B **59**, 15 033 (1999).
[59] A. F. Guillermet and G. Grimvall, Phys. Rev. B **40**, 1521 (1989).
[60] S. V. Meschel and O. J. Kleppa, Metall. Trans. A **24**, 947 (1993).
[61] L. A. Reznitskii, Russ. J. Phys. Chem. **41**, 612 (1967).
[62] J. H. Rose, J. Ferrante, and J. R. Smith, Phys. Rev. Lett. **47**, 675 (1981).
[63] J. R. Smith, J. Ferrante, and J. H. Rose, Phys. Rev. B **31**, 3427 (1985).
[64] J. Ferrante, J. R. Smith, and J. H. Rose, Phys. Rev. B **28**, 1835 (1983).
[65] P. Vinet, J. H. Rose, J. Ferrante, and J. R. Smith, J. Phys.: Condens. Matter **1**, 1941 (1989).
[66] F. D. Murnaghan, Proc. Natl. Acad. Sci. U.S.A. **30**, 244 (1944).
[67] P. Ravindran and R. Asokamani, Phys. Rev. B **53**, 1129 (1996).
[68] C. Ravi, P. Vajeeston, S. Mathijaya, and R. Asokamani, Phys. Rev. B **60**, 15 683 (1999).
[69] A. K. McMahan, H. L. Skriver, and B. Johansson, in *Physics of Solids Under High Pressures*, edited by J. Schilling and R. N. Shelton (North-Holland, Amsterdam, 1981), p. 169.
[70] F. Mulargia and F. Quareni, Geophys. J. **92**, 269 (1988).
[71] S. Raju, E. Mohandas, and V. S. Raghunathan, J. Phys. Chem. Solids **58**, 1367 (1997).
[72] B. T. Matthias, Prog. Low Temp. Phys. **2**, 138 (1957).
[73] L. Leyarovska and E. Leyarovski, J. Less-Common Met. **67**, 249 (1979).
[74] S. Funahashi, Y. Hamaguchi, T. Tanaka, and E. Bannai, Solid State Commun. **23**, 859 (1977).
[75] L. Andersson, B. Dellby, and H. P. Myers, Solid State Commun. **4**, 77 (1966).
[76] N. Lundquist, H. P. Myers, and P. Westin, Philos. Mag. **7**, 1187 (1962).
[77] J. Samuel and Jr. Schneider, *ASM Engineering Materials Hand Book*, Vol. 4 (ASM International, Materials Park, OH, 1991), pp. 790–795.
[78] M. Weinert and R. E. Watson, Phys. Rev. B **58**, 9732 (1998).